

Impinging flow of a special third-grade nanofluid streaming over a porous receding sheet using the tri-temperature model

PALANISAMY GAYATHRI 1 $^{\odot}$, NAGARAJAN NITHYADEVI 2 , KRISHNAN SATHYASRI 3 and NARAMGARI SANDEEP 4

MS received 16 November 2023; revised 14 April 2024; accepted 26 April 2024

Abstract. The heat transfer characterisation of the three-phase local thermal non-equilibrium analysis due to the nanofluid (solid particle phase and the base fluid phase) and the absorbing phase (due to the porous surface) is performed for a third-grade nanofluid impinging over a receding surface. The mathematical formulation of the physical model includes the Rivlin-Ericksen tensor for fluids of grade three with appropriate restriction to viscous flows and also incorporates the Buongiorno nanofluid model for studying the impact of thermophoresis and Brownian motion. The resultant governing time-dependent partial differential equations has been converted to ordinary differential equations by applying similarity transformation. The computational results are obtained using the finite-difference approach in the Matlab software. The non-Newtonian and the time-dependent flow phenomena demands an additional boundary condition to ensure the uniqueness of the solution. With a general third-grade assumption with the wall shrinking and unsteadiness, the resultant equations govern the occurrence of dual solution in the obtained numerical results. The stability investigation reports the existence of multiple (dual) solutions due to the unsteadiness imparted in the flow and the flow behaviour of both the stable and unstable solutions are revealed. The boundary layer characteristics are explored for various vital physical parameters, such as material parameter, porous permeability parameter, Brownian motion parameter, thermophoresis parameter, inter-phase heat transfer coefficient, modified thermal capacity ratio, modified thermal diffusivity ratio and buoyancy ratio parameter. The temperature distribution across different phases is analysed for the stable solutions.

Keywords. Stagnation point; thermal non-equilibrium; third-grade nanofluid; shrinking surface.

PACS Nos 47.15.-x; 47.55.pb; 47.56.+r

1. Introduction

The study of fluid flow in absorbing mediums has become an area of vital importance, as the results are useful in multitudinous technological applications, including microwave heating, microelectronics cooling, fibrous insulation, buildings insulation, gas filtration in automobiles, etc. An appropriate mathematical modelling and the computing results of the flow through porous materials is done using many factors like particle or pore shape, the type of the porous material, the characteristic temperature of the fluid and solid matrix, the solid matrix temperature, speed of fluid flow, etc. In many cases, the fluid-drenched porous medium abides

the local thermal equilibrium (LTE), which means that the temperature distinction between the characteristic temperature of the fluid and solid matter is of infinitesimal order. Several situations arise in solid matrix heat exchangers, nuclear reactor construction, etc., where the difference between the average fluid phase and solid phase temperature will be significant. An experimental study on the heat and fluid flow in a plate channel operated with metallic or non-metallic particles was executed by Jiang et al [1]. Their comparative analysis of the experimental and computational results disclosed the fact that in metallic porous structures, thermal non-equilibrium approach in the computations produced more accurate results than the equilibrium approach.

¹Department of Mathematics, PSG College of Arts & Science, Coimbatore 641 014, India

²Department of Applied Mathematics, Bharathiar University, Coimbatore 641 046, India

³Department of Mathematics, GITAM University, Visakhapatnam 530045, India

⁴Department of Mathematics, Central University of Karnataka, Kalaburagi 585 367, India

^{*}Corresponding authors. E-mail: gayathri08psg@gmail.com; nithyadevin@gmail.com

Local thermal non-equilibrium (LTNE) transport of heat (or poroelasticity approach) assumes that the thermal energy is transmitted from fluid to solid phase at a microscopic level and thence, a non-negligible difference in temperature occurs between the fluid and solid phase in the porous medium. Thermal nonequilibrium approach has been employed by several investigators [2–10] during the last few decades for various flow geometries. Nouri-Borujerdi et al [2] applied the LTNE inside the porous medium with externally applied heat generation. Wu et al [3] adopted LTNE model to study the convective flow and heat transfer within a rectangular cavity with heat-producing porous structure. They showed that the heat transfer of the porous medium was decreased with increasing interphase thermal transmission coefficient. Omara et al [4] numerically investigated the LTNE state in a thermosolutal convective flow. The impact of the electromagnetic field on temperature, concentration and velocity field in porous media was analysed by Montienthong et al [5]. Their analysis revealed the existence of a larger difference in temperature between the solid and fluid phases. The implication of heat energy radiating processes generated by virtue of the fluid moving through porous media was investigated using LTNE approach by Chen et al [6]. Computational results of the entropy generation due to an impinging jet acting over a porous sink assuming thermal nonequilibrium was investigated by Salimi et al [7]. The LTNE model for heat emissive porous medium was explored with side cooling approach by Chakravarty et al [8]. A comprehensive review with an associated comparison between the LTE approach and LTNE one for different porous structures was examined by Pati et al [9]. Their survey suggested to deploy LTNE approach with various effects such as magnetic forces, radiative effects, etc. The pore scale simulations for the local thermal equilibrium (LTE) and (LTNE two-temperature approach) in phase changing and melting materials was performed by Nemati et al [10].

The core region of any impinging fluid flow field at which the velocity of the fluid vanishes represents a stagnation point. Hiemenz [11] discovered that the Navier–Stokes equation can be used for analysing the viscous regions in the neighbourhood of the stagnation region. Khan and Pop [12] adopted the two-temperature model for exploring heat transfer over a planar stagnation region. The influence of flow separation confined in a stagnation region subject to wall stretching is analysed by Sadiq *et al* [13].

Recent researchers and industrialists are switching from using typical heat conducting fluids or coolants, such as the engine oil, water, ethylene glycol, etc., to the contemporary nanofluids. Nanofluids form a powerful tool in heat transferring applications, such as the heating and ventilation devices, cooling of heavy engine automobile systems, in food processing systems, etc. Nanoparticles may also pave the way for practical and renewable energy. Specifically, nanofluids can be used as a powerful tool for transferring heat from solar energy collectors to their storage tanks. Nanofluids are of paramount significance in diverse fields, such as electrochemical and thermal engineering, food processing, sustainable energy, in automotive industries, etc. [14,15]. Gomari et al [16] numerically simulated the viscous layers bounding to the stagnation flow of the nanofluid streaming around a cylinder and predicted the entropy generated during the heat transfer process. The boron nitrate composite-based nanofluid flow within a curved microchannel with electro-osmotic effects were examined by Akram et al [17]. Mandal et al [18] focussed on carbon-based nanofluid impinging flows with an enlarging/shrinking viscous layers. The ternary nanofluid with electro-osmosis effects are investigated by Prakash et al [19]. Waini et al [20] obtained symmetrical solutions of the steady-state planar stagnation region of the hybrid nanofluid. The optimisation of the fluid flow over a rotating sphere with conjugate nonlinear convection-radiation process was performed by Rana *et al* [21].

The nanofluid flow in an embedded porous medium using a three temperature model was pioneered by Kuznetsov and Nield [22]. This temperature model constitutes the solid phase of the porous medium, the nanoparticle phase and the fluid phase. Bhadauria and Agarwal [23] inspected the existence of stable solutions in a nanofluid drowned porous medium with LTNE assumption.

The non-Newtonian fluids are actively used in many contemporary appliances in the domain of geophysics, material processing, etc. The viscoplastic (non-Newtonian) nanofluid flow past stenosed arteries are examined and the results of this study is said to be applicable in human circulatory systems [24]. Specifically, the non-Newtonian fluids of differential types of grade *n* has been of special interest for the past few decades. The viscoelastic effects exhibited with regard to the motion of second-grade fluids was investigated extensively by many researchers [25,26]. They showed that the application of these kind of problems can be found in extrusion of polymer from a die. Prakash *et al* [27] investigated the electromagnetohydrodynamic flow characteristics of ionic nanofluids driven by peristalsis.

Second-grade fluid possesses the normal stress effects and lacks the ability to account for viscous thining/ thickening attributes which can be counterfeited by using the third-grade flow analysis. Following this, many studies have been carried out for the flow of third-grade fluids [28–31]. Abbasbandy and Hayat [28] obtained the solutions of a special third-grade fluid in semi-analytical form. The flow of third-grade fluid subject to peristaltic effects due to the contraction and dilation processes with varying thermal conductivity ratio was analysed by Hayat *et al* [29]. Chu *et al* [30] examined the impact of the third-grade fluid with Brownian motion exhibited by the gyrostatic microorganisms dispersed inside third-grade fluids. Ogunsola *et al* [31] studied the energy loss through the entropy generated in chemical processes coupled with the Arrhenius energy.

The nanofluid modelling based on two distinctive phases constituting the solid phase and the fluid phase for distinct flow domains was done by Turkyilmazoglu [32]. Triple diffusive convection phenomena in nanofluids considering the stabilising and destabilising effects over a diverse range of Lewis number and Reynolds number was simulated by Shukla and Gupta [33] using the Galerkin procedure.

Thus, the main objective of this study relies on examining the viscous layers associated with the stable solutions of the stagnation point flow of nanofluid past a porous shrinking surface. The governing flow attributes to the formation of stagnation zones with the thermal non-equilibrium due to the tri-temperature phases (fluid, solid and the nanoparticle). To the best of the authors' knowledge, the study of an unsteady stagnation point flow of a third-grade nanofluid past a porous shrinking surface using the local thermal non-equilibrium model among the particle, fluid and solid-matrix phases is a research to be considered. The obtained solutions will be analysed for the existence of stable solutions among the obtained multiple solutions.

2. Formulation of the problem

Consider an unsteady, incompressible impinging viscous flow of special third-grade nanofluid ascribed in the neighbourhood of a planar stagnation region. The flow is modelled in the Cartesian coordinates (x, y) with the resulting velocity variables symbolised as (u, v) (see figure 1). The horizontal plane is subjected to move towards the origin by applying two equal forces and the sheet is shrunk with a time-dependent velocity $U_w = \lambda u_w$ ($\lambda < 0$ is the shrinking rate and $\lambda > 0$ is the stretching rate). Thus, a moving porous surface (with porosity ϵ and coinciding with the plane y = 0) is aligned with a uniform, time-dependent speed u_∞ and moving along the opposite direction of the stream. The time- and space-dependent solid-phase temperature is given by

$$T_w = T_\infty + \frac{bx}{1 - ct},$$

where b>0 governs the assisting flow and b<0 governs opposing flow. The ambient fluid and the fluid adjacent to the stagnation wall are T_w and T_∞ , while the ambient and the wall adjacent nanoparticle volume fraction are ϕ_w and ϕ_∞ , respectively. The fluid saturated porous medium is assumed to be homogeneous. The flow near the stagnation region is slow and hence the terms representing advection and Forchheimer quadratic resistance with regard to the flow drag is neglected. The considered planar flow region comprised of a homogeneous porous material is damped in a nanofluid.

The flow has an incompressible behaviour with nonnegligible density transitions due to the Boussinesq approximation and all other fluid properties remain invariant.

The stress constitutive equation for the differential fluid of third grade is given by Fosdick and Rajagopal [34] in the following form:

$$\tau = -pI + \mu A_1 + \alpha_1 A_1 + \alpha_2 A_1^2 + \beta_1 A_3 + \beta_2 (A_1 A_2 + A_2 A_1) + \beta_3 (\text{tr} A_1^2) A_1,$$
 (1)

where p is the spherical pressure, I accounts for the identity tensor and μ is the dynamic viscosity. The third-grade material parameters β_1 and β_2 are assumed to vanish. The first two Rivlin–Ericksen tensors A_1 and A_2 can be written as

$$A_1 = (\nabla \mathbf{u}) + (\nabla \mathbf{u})^T,$$

$$A_2 = \frac{\mathrm{d}A_1}{\mathrm{d}t} + A_1(\nabla \mathbf{u}) + (\nabla \mathbf{u})^t A_1.$$
(2)

Moreover, the viscous stress coefficients α_1 , and β_3 are non-negative constants and the material parameters are entitled to satisfy the thermodynamic constraints:

$$\alpha_1 + \alpha_2 \le \sqrt{24\alpha\beta_3}.\tag{3}$$

Following [28,35], the second-grade terms in the third-grade fluid formulation are neglected compared to the viscous terms. The three-temperature phase equations follow from Bhaduaria and Agarwal [23]. The governing boundary layer equations follows from Abbasbandy and Hayat [28].

Continuity equation

$$\frac{\partial u}{\partial x} + \frac{\partial v}{\partial y} = 0. {4}$$

Momentum equation

$$\frac{\rho_f}{\epsilon} \frac{\partial u}{\partial t} + \frac{\rho_f}{\epsilon^2} \left(u \frac{\partial u}{\partial x} + v \frac{\partial u}{\partial y} \right)$$

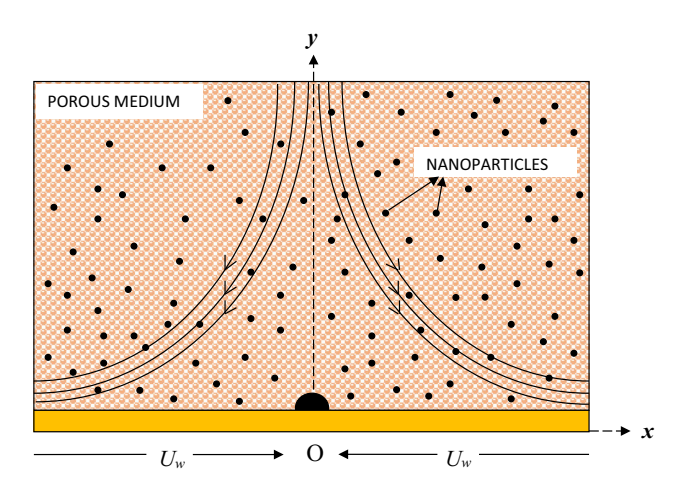


Figure 1. Schematic configuration of the stagnation point flow impinging over a flat surface.

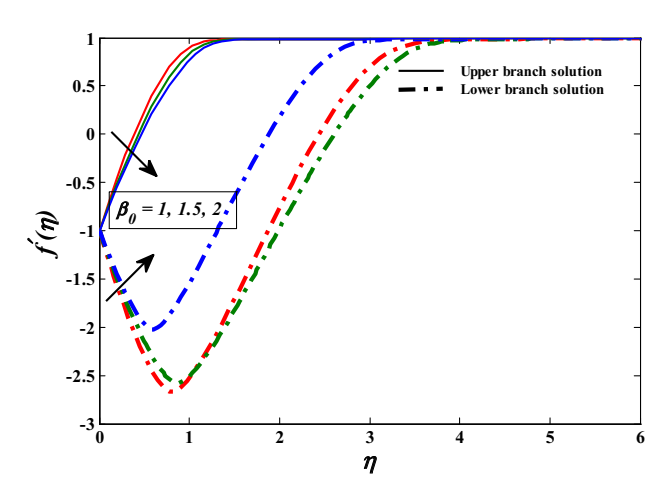


Figure 2. Effect of material parameter β_0 on the velocity profile when $\gamma_p = \gamma_s = \epsilon_p = \epsilon_s = N_{HS} = N_{HP} = 1, Nb = Nt = Nr = 0.1, \lambda = A = -1, s = Le = Pr = 1 and <math>\Lambda = 2$.

$$= \frac{\partial u_{\infty}}{\partial t} + u_{\infty} \frac{\partial u_{\infty}}{\partial x} + \mu_{f} \frac{\partial^{2} u}{\partial y^{2}} + 6k \left(\frac{\partial u}{\partial y}\right)^{2} \frac{\partial^{2} u}{\partial y^{2}} - \frac{\mu}{K'} (u - u_{\infty}) + [(1 - \phi_{\infty})\rho_{f\infty}\beta(T_{f} - T_{\infty}) - (\rho_{p} - \rho_{f\infty})(\phi - \phi_{\infty})]g.$$
 (5)

Temperature equation for the fluid phase

$$\begin{split} &\epsilon (1-\phi_{\infty})(\rho C)_{f} \left[\frac{\partial T_{f}}{\partial t} + \frac{1}{\epsilon} \left(u \frac{\partial T_{f}}{\partial x} + v \frac{\partial T_{f}}{\partial y} \right) \right] \\ &= \epsilon (1-\phi_{\infty}) k_{f} \frac{\partial^{2} T_{f}}{\partial y^{2}} + \epsilon (1-\phi_{\infty})(\rho C)_{p} \\ &\times \left[D_{B} \frac{\partial \phi}{\partial y} \frac{\partial T_{f}}{\partial y} + \frac{D_{T}}{T_{\infty}} \left(\frac{\partial T_{f}}{\partial y} \right)^{2} \right] + h_{fp} (T_{p} - T_{f}) \\ &+ h_{fs} (T_{s} - T_{f}). \end{split}$$

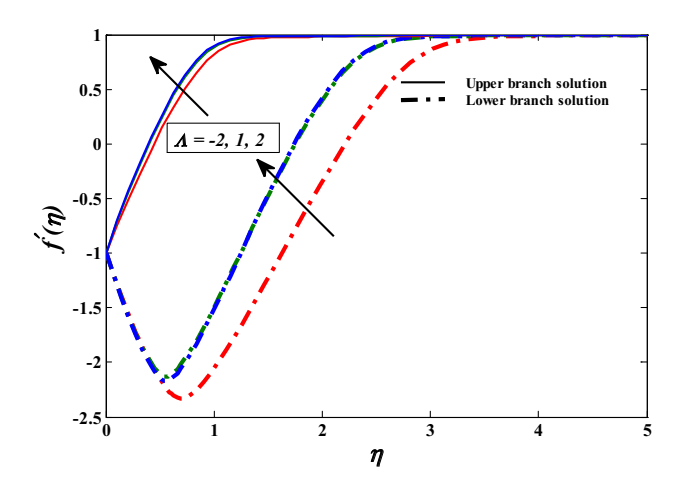


Figure 3. Effect of porous permeability parameter Λ on the velocity profile when $\gamma_p = \gamma_s = \epsilon_p = \epsilon_s = N_{HS} = N_{HP} = 1, Nb = Nt = Nr = 0.1, \lambda = A = -1$ and $\beta_0 = s = Le = Pr = 1$.

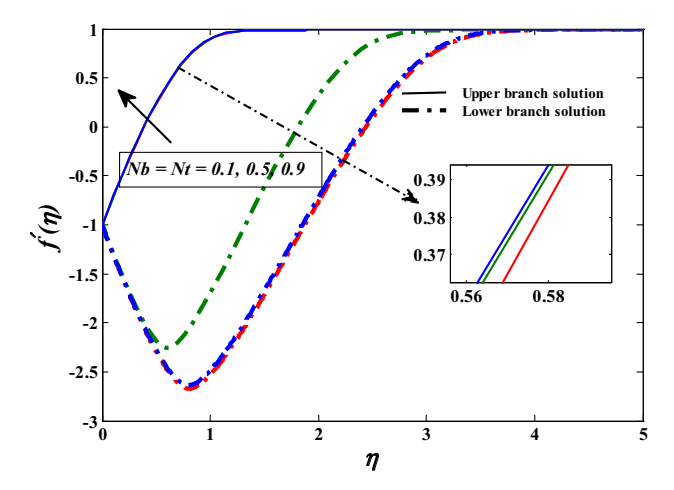


Figure 4. Effect of Brownian diffusion parameter Nb and thermophoresis parameter Nt on the velocity profile when $\gamma_p = \gamma_s = \epsilon_p = \epsilon_s = N_{HS} = N_{HP} = 1, Nr = 0.1, \lambda = A = -1, \beta_0 = s = Le = Pr = 1$ and $\Lambda = 2$.

Temperature equation for the particle phase

$$\epsilon \phi_{\infty}(\rho C)_{p} \left[\frac{\partial T_{p}}{\partial t} + \frac{1}{\epsilon} \left(u \frac{\partial T_{p}}{\partial x} + v \frac{\partial T_{p}}{\partial y} \right) \right]$$

$$= \epsilon \phi_{\infty} k_{p} \frac{\partial^{2} T_{p}}{\partial y^{2}} - h_{fp} (T_{p} - T_{f}). \tag{7}$$

Temperature equation for the solid phase

$$(1 - \epsilon)(\rho C)_s \frac{\partial T_s}{\partial t} = (1 - \epsilon)k_s \frac{\partial^2 T_s}{\partial y^2} - h_{fs}(T_s - T_f).$$
(8)

Nanoparticle volume fraction equation

(6)
$$\frac{\partial \phi}{\partial t} + \frac{1}{\epsilon} \left(u \frac{\partial \phi}{\partial x} + v \frac{\partial \phi}{\partial y} \right) = D_B \frac{\partial^2 \phi}{\partial y^2} + \frac{D_T}{T_\infty} \frac{\partial^2 T_f}{\partial y^2}. \quad (9)$$

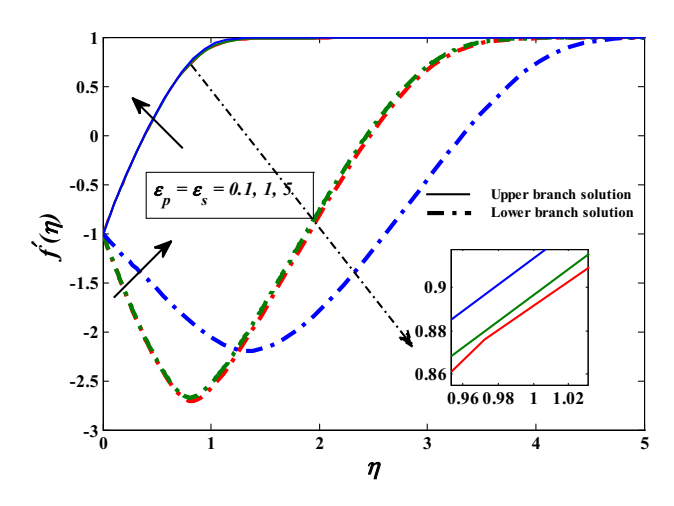


Figure 5. Effect of the modified diffusivity ratios ϵ_p and ϵ_s of the particle and solid phases on the velocity profile when $\gamma_p = \gamma_s = N_{HS} = N_{HP} = 1$, Nr = Nb = Nt = 0.1, $\lambda = A = -1$, $\beta_0 = s = Le = Pr = 1$ and $\Lambda = 2$.

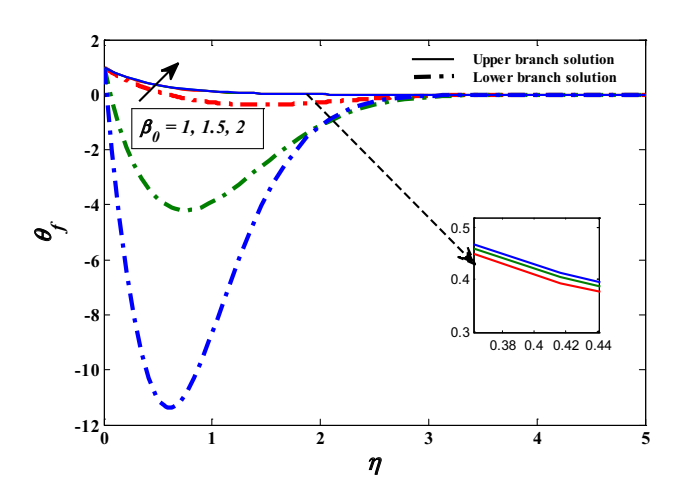


Figure 6. Effect of material parameter β_0 on the temperature profile of the fluid phase when $\gamma_p = \gamma_s = \epsilon_p = \epsilon_s = N_{HS} = N_{HP} = 1$, Nb = Nt = Nr = 0.1, $\lambda = A = -1$, s = Le = Pr = 1 and $\Lambda = 2$.

The governing physical model follows the boundary conditions:

At
$$y = 0$$
: $u = U_w = -\lambda u_w$, $v = v_w$,
 $T_f = T_w$, $T_p = T_w$, $T_s = T_w$, $\phi = \phi_w$
As $y \to \infty$: $u \to u_\infty$, $T_f \to T_\infty$, (10)
 $T_p \to T_\infty$, $T_s \to T_\infty$, $\phi \to \phi_\infty$,

where u and v symbolise the velocity along the x and y directions, ρ_f and β correspond to the viscosity and volumetric expansion coefficient of the fluid, respectively. The heat capacities of the fluid, nanoparticle and solid phases are represented as $(\rho c)_f$, $(\rho c)_p$, $(\rho c)_s$ and their respective thermal conductivities are k_f , k_p , k_s , respectively.

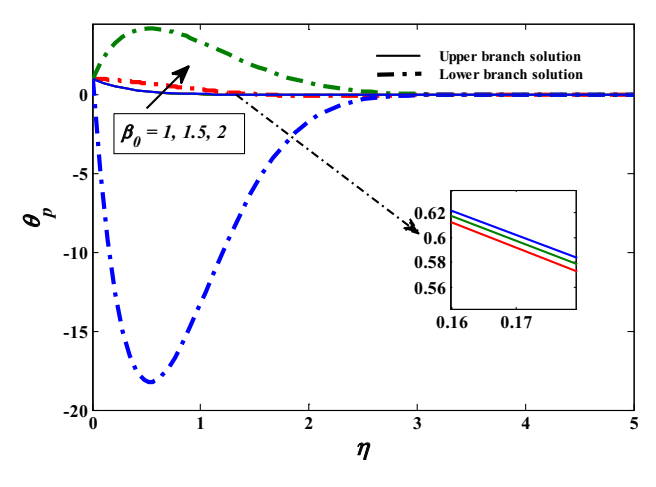


Figure 7. Effect of material parameter β_0 on the temperature profile of the particle phase when $\gamma_p = \gamma_s = \epsilon_p = \epsilon_s = N_{HS} = N_{HP} = 1$, Nb = Nt = Nr = 0.1, $\lambda = A = -1$, s = Le = Pr = 1 and $\Lambda = 2$.

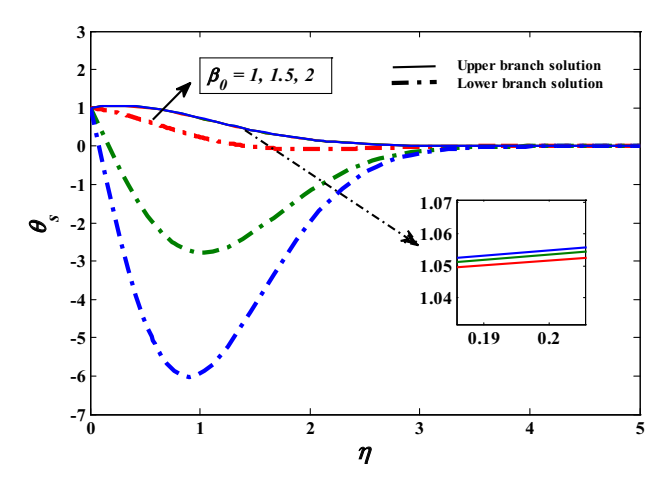


Figure 8. Effect of material parameter β_0 on the temperature profile of the solid phase when $\gamma_p = \gamma_s = \epsilon_p = \epsilon_s = N_{HS} = N_{HP} = 1$, Nb = Nt = Nr = 0.1, $\lambda = A = -1$, s = Le = Pr = 1 and $\Lambda = 2$.

The coefficients D_B and D_T signify the Brownian motion and the thermophoretic diffusion coefficients, while the interface heat transfer coefficients due to the fluid–particle and the fluid–solid interphases are expressed as h_{fp} and h_{fs} , respectively.

The velocity of the inviscid fluid is given by

$$u_{\infty} = u_w = \frac{ax}{1 - ct}. (11)$$

To simplify the problem, dimensionless functions f, θ_f , θ_p , θ_s , Φ are introduced:

$$\eta = y \sqrt{\frac{a}{\nu_f (1 - ct)}}, \quad \psi = \sqrt{\frac{a\nu_f}{1 - ct}} x f(\eta),$$

$$\theta_f = \frac{T_f - T_\infty}{T_w - T_\infty}, \quad \theta_p = \frac{T_p - T_\infty}{T_w - T_\infty},$$

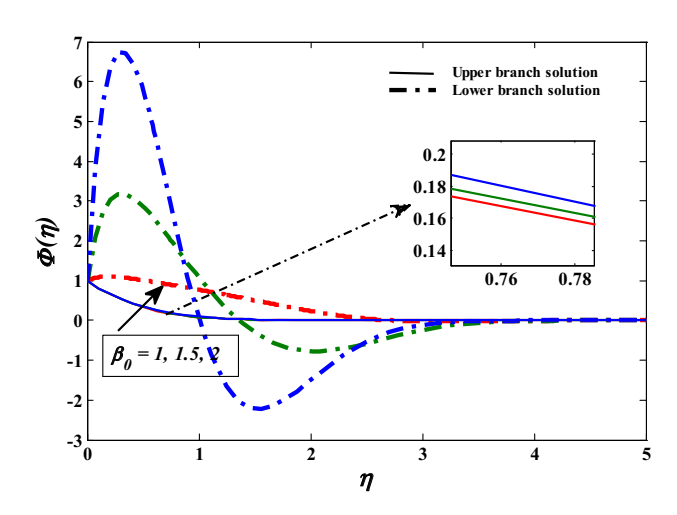


Figure 9. Effect of material parameter β_0 on mass concentration distribution when $\gamma_p = \gamma_s = \epsilon_p = \epsilon_s = N_{HS}$ $= N_{HP} = 1$, Nb = Nt = Nr = 0.1, $\lambda = A = -1$, s = Le = Pr = 1 and $\Lambda = 2$.

$$\theta_s = \frac{T_s - T_{\infty}}{T_w - T_{\infty}}, \quad \Phi = \frac{\phi - \phi_{\infty}}{\phi_w - \phi_{\infty}}.$$
 (12)

Substituting eqs (11) and (12) into eqs (4)–(9), the resulting mathematical model follows:

$$f'''(1+\beta_{0}f''^{2})+1+A+\Lambda(1-f')+Ri(\theta_{f}-Nr\Phi)$$

$$-\frac{A}{\epsilon}\left(f'+\frac{\eta}{2}f''\right)-\frac{1}{\epsilon^{2}}\left(f'^{2}-ff''\right)=0, \qquad (13)$$

$$\frac{1}{Pr}\theta''_{f}-\frac{A\eta}{2}\theta'_{f}+Nb\theta'_{f}\Phi'+\frac{1}{\epsilon}f\theta'_{f}-\frac{1}{\epsilon}f'\theta_{f}-A\theta_{f}$$

$$+Nt\theta'_{f}^{2}+N_{HP}(\theta_{p}-\theta_{f})+N_{HS}(\theta_{s}-\theta_{f})=0, \qquad (14)$$

$$\frac{\epsilon_{p}}{Pr}\theta_{p}^{"} - \frac{A\eta}{2}\theta_{p}^{'} + \frac{1}{\epsilon}f\theta_{p}^{'} - \frac{1}{\epsilon}f^{'}\theta_{p} - A\theta_{p} - \gamma_{p}N_{HP}(\theta_{p} - \theta_{f}) = 0, \tag{15}$$

$$\frac{\epsilon_s}{Pr}\theta_s'' - A\frac{\eta\theta_s'}{2} - A\theta_s - \gamma_s N_{HS}(\theta_s - \theta_f) = 0, \quad (16)$$

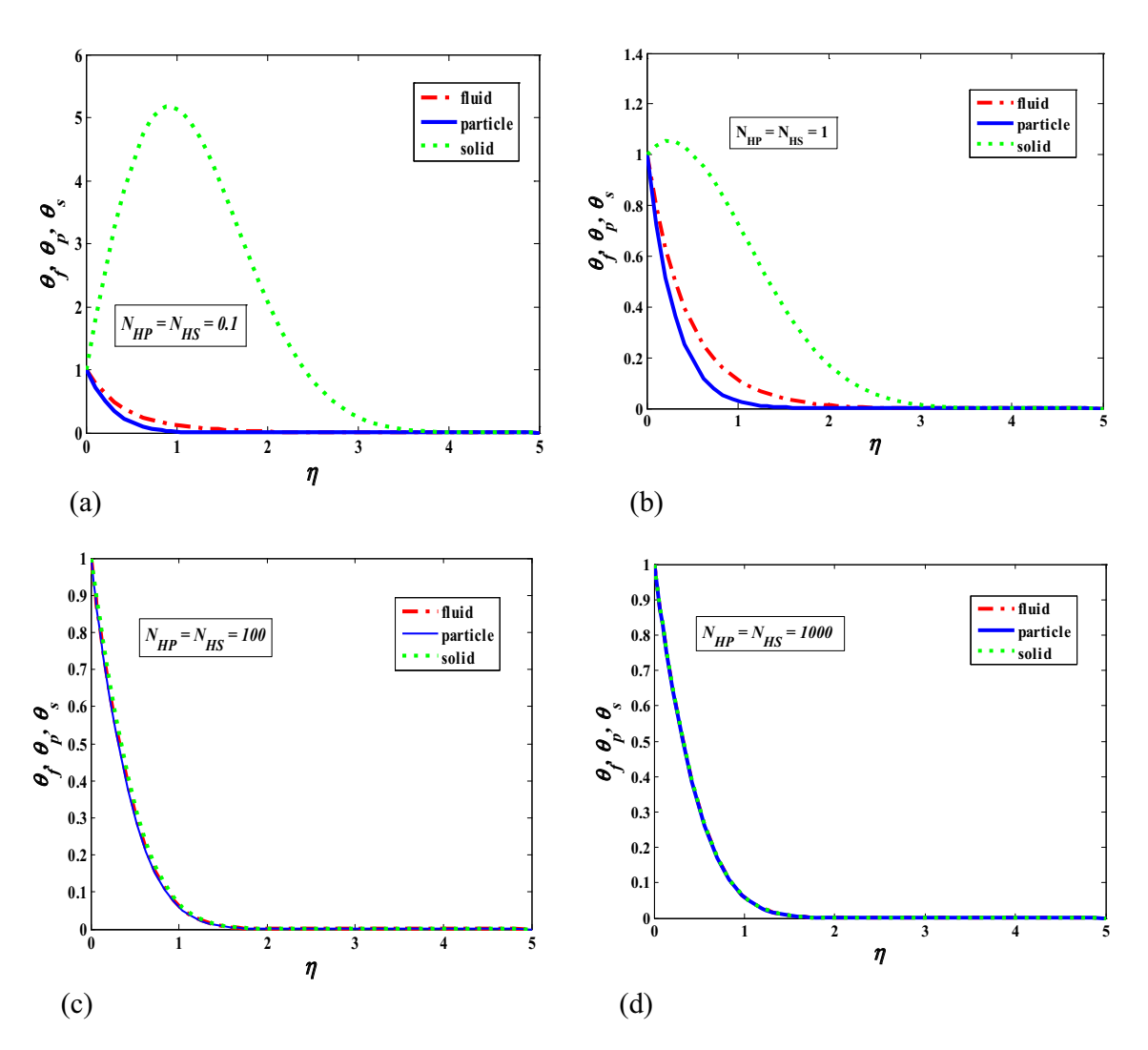


Figure 10. Effect of Nield numbers N_{HP} and N_{HS} on the temperature profile when $\gamma_p = \gamma_s = \epsilon_p = \epsilon_s = 1$, Nb = Nt = Nr = 0.1, $\lambda = A = -1$, s = Le = Pr = 1 and $\Lambda = 2$.

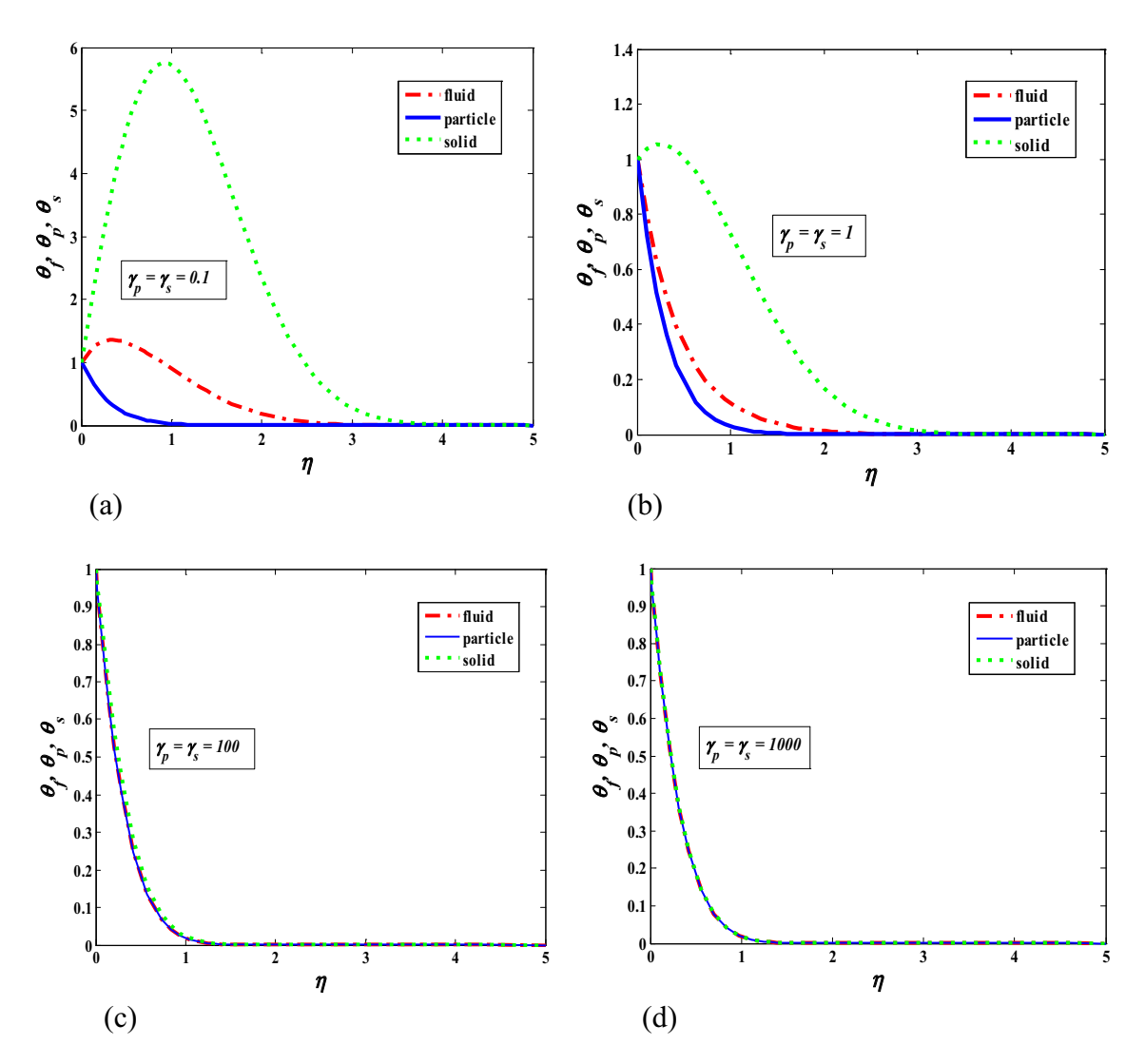


Figure 11. Effect of modified capacity ratios γ_p and γ_s on the temperature profile when $\gamma_p = \gamma_s = N_{HS} = N_{HP} = 1$, Nb = Nt = Nr = 0.1, $\lambda = A = -1$, s = Le = Pr = 1 and $\Lambda = 2$.

$$\frac{1}{Le}\left(\Phi'' + \frac{Nt}{Nb}\theta_f''\right) - \frac{A\eta}{2}\Phi' + \frac{1}{\epsilon}f\Phi' = 0, \tag{17}$$

with accompanied boundary conditions (eq. (11))

At
$$\eta = 0$$
: $f = 0$, $f' = \lambda$, $\theta_f = 1$,
 $\theta_p = 1$, $\theta_s = 1$, $\Phi = 1$. (18)
As $\eta \to \infty$: $f' \to 1$, $\theta_f \to 0$, $\theta_p \to 0$,
 $\theta_s \to 0$, $\Phi \to 0$,

where the third-grade parameter

$$\beta_0 = 6k_0a^3/v_f^2$$

the Prandtl number

$$Pr = \frac{v_f}{\alpha_f},$$

the Lewis number,

$$Le = \frac{\gamma}{D_B},$$

the Grashof number

$$Gr = \frac{g\beta(T_w - T_\infty)x^3}{v_f^2},$$

the Reynolds number

$$Re_x = \frac{u_{\infty}x}{v_f},$$

the buoyancy ratio parameter

$$Nr = \frac{(\rho_p - \rho_{f\infty})(\phi_w - \phi_\infty)}{(1 - \phi_\infty)\rho_{f\infty}\beta(T_w - T_\infty)},$$

the unsteadiness parameter

$$A = c/a$$

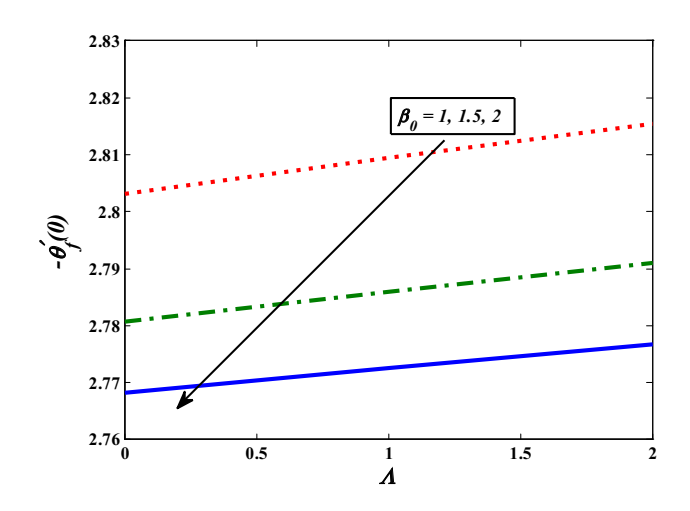


Figure 12. Effect of material parameter β_0 for varying Λ on the reduced Nusselt number of the fluid phase when $\gamma_p = \gamma_s = \epsilon = \epsilon_s = N_{HS} = N_{HP} = 1, Nb = Nt$ = $Nr = 0.1, \lambda = A = -1, s = Le = Pr = 1.$

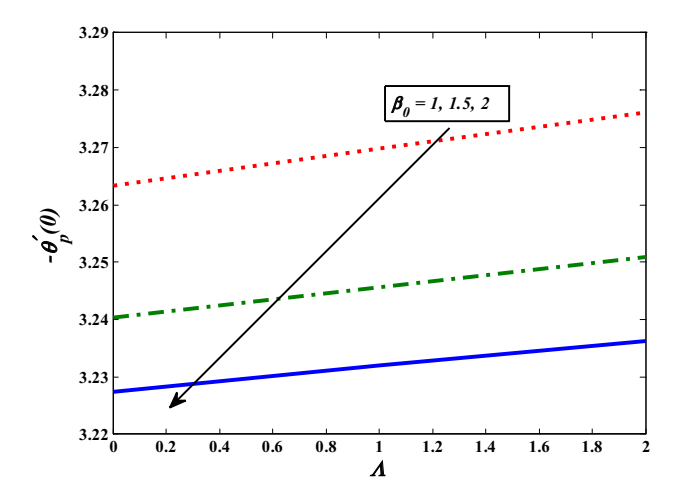


Figure 13. Effect of material parameter β_0 for varying Λ on the reduced Nusselt number of the particle phase when $\gamma_p = \gamma_s = \epsilon_p = \epsilon_s = N_{HS} = N_{HP} = 1, Nb = Nt$ = $Nr = 0.1, \lambda = A = -1, s = Le = Pr = 1.$

the porous permeability parameter

$$\Lambda = \frac{v_f x}{K u_\infty},$$

the modified diffusivity ratios

$$\epsilon_p = \frac{\alpha_p}{\alpha_f}$$
 and $\epsilon_s = \frac{\alpha_s}{\alpha_f}$,

the modified capacity ratios

$$\gamma_p = \frac{(1 - \phi_\infty)(\rho C)_f}{\phi_\infty(\rho C)_p} \text{ and } \gamma_s = \frac{\epsilon (1 - \phi_\infty)(\rho C)_f}{(1 - \epsilon)(\rho C)_s}, \qquad Nb = \frac{(\rho C)_p D_B(\phi_w - \phi_\infty)}{(\rho C)_f \nu_f}$$

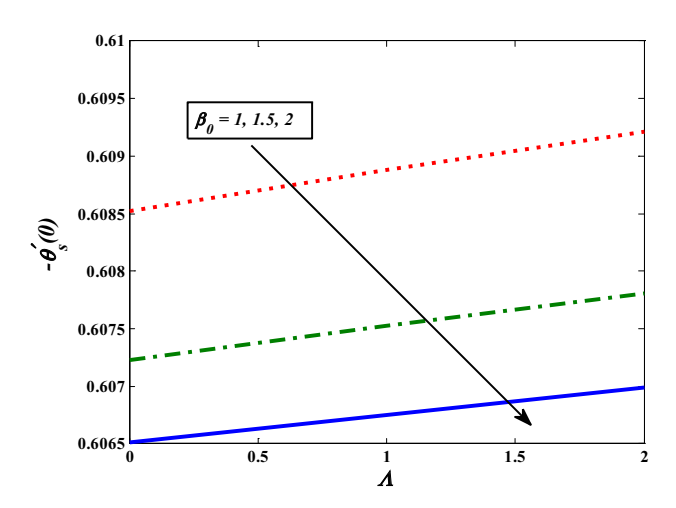


Figure 14. Effect of material parameter β_0 for varying Λ on the reduced Nusselt number of the solid phase when $\gamma_p = \gamma_s = \epsilon_p = \epsilon_s = N_{HS} = N_{HP} = 1$, Nb = Nt = Nr = 0.1, $\lambda = A = -1$, s = Le = Pr = 1.

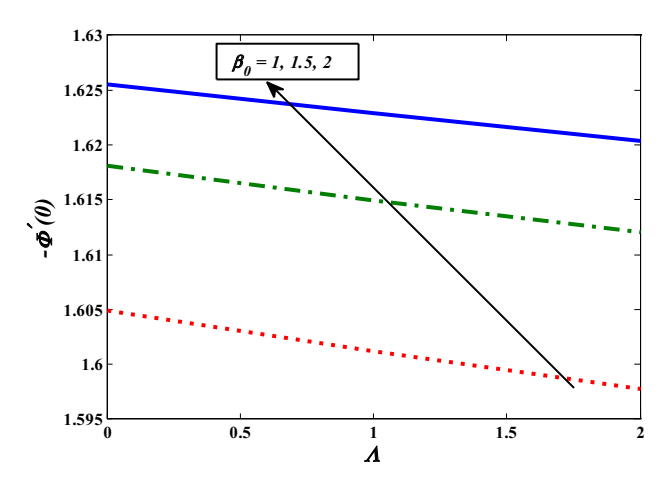


Figure 15. Effect of material parameter β_0 for varying Λ on Sherwood number when $\gamma_p = \gamma_s = \epsilon_p$ = $\epsilon_s = N_{HS} = N_{HP} = 1$, Nb = Nt = Nr = 0.1, Nb = Nt = Nr = 0.1, $\lambda = A = -1$, $\lambda = A = -1$, $\lambda = A = -1$.

the Nield numbers

$$N_{HP} = \frac{h_{fp} x \alpha_f}{\epsilon (1 - \phi_{\infty}) k_f u_{\infty}}$$
 and $N_{HS} = \frac{h_{fs} x \alpha_f}{\epsilon (1 - \phi_{\infty}) k_f u_{\infty}}$,

the Richardson number

$$Ri = \frac{Gr}{Re_r^2},$$

the Brownian diffusion

$$Nb = \frac{(\rho C)_p D_B(\phi_w - \phi_\infty)}{(\rho C)_f v_f}$$

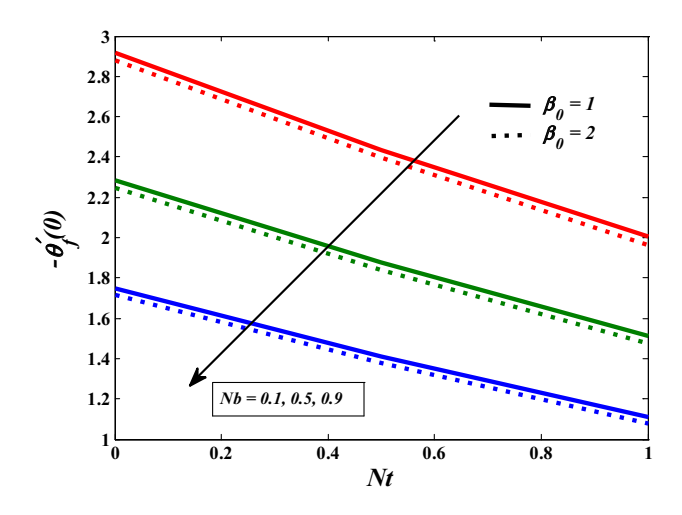


Figure 16. Effect of Brownian diffusion parameter Nb and thermophoresis parameter Nt on the reduced Nusselt number of the fluid phase when $\gamma_p = \gamma_s = \epsilon_p = \epsilon_s = N_{HS} = N_{HP} = 1, Nr = 0.1, \lambda = A = -1, s = Le = Pr = 1$ and $\Lambda = 2$.

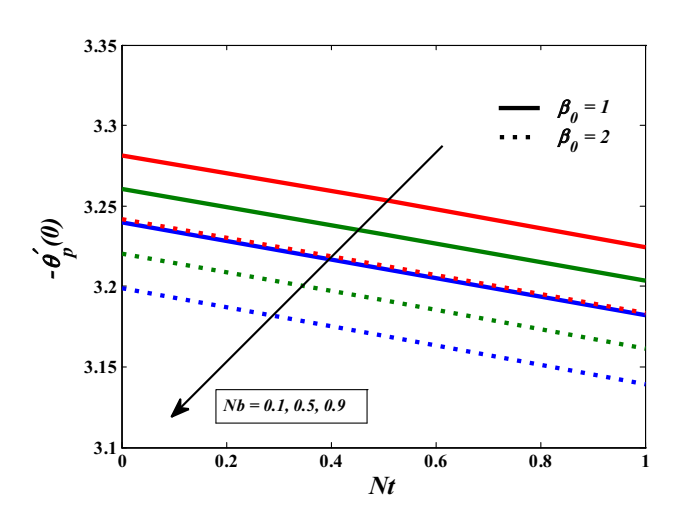


Figure 17. Effect of Brownian diffusion parameter Nb and thermophoresis parameter Nt on the reduced Nusselt number of the particle phase when $\gamma_p = \gamma_s = \epsilon_p = \epsilon_s = N_{HS} = N_{HP} = 1, Nr = 0.1, \lambda = A = -1, s = Le = Pr = 1$ and $\Lambda = 2$.

and thermophoresis parameter

$$Nt = \frac{(\rho C)_p D_T (T_w - T_\infty)}{(\rho C)_f T_\infty \nu_f}.$$

The skin-friction coefficient C_f , the local Nusselt numbers for the fluid, particle, solid-matrix phases Nu_f , Nu_p , Nu_s and the local Sherwood number Sh follow:

$$C_f = \frac{\tau_w}{\rho u_\infty^2}, \quad Nu_f = \frac{x(q_w)_f}{k_f(T_w - T_\infty)},$$

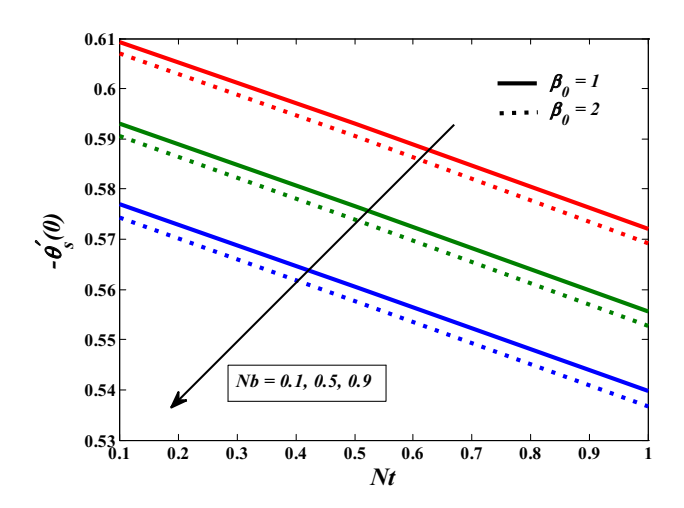


Figure 18. Effect of Brownian diffusion parameter Nb and thermophoresis parameter Nt on the reduced Nusselt number of the fluid phase when $\gamma_p = \gamma_s = \epsilon_p = \epsilon_s = N_{HS} = N_{HP} = 1, Nr = 0.1, \lambda = A = -1, s = Le = Pr = 1$ and $\Lambda = 2$.

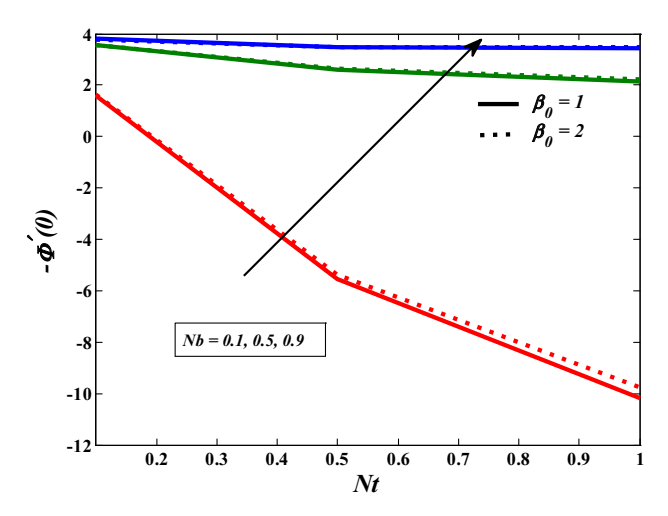


Figure 19. Effect of Brownian diffusion parameter Nb and thermophoresis parameter Nt on the reduced Nusselt number of the fluid phase when $\gamma_p = \gamma_s = \epsilon_p = \epsilon_s = N_{HS} = N_{HP} = 1, Nr = 0.1, \lambda = A = -1, s = Le = Pr = 1$ and $\Lambda = 2$.

$$Nu_p = \frac{x(q_w)_p}{k_p(T_w - T_\infty)}, \quad Nu_s = \frac{x(q_w)_s}{k_s(T_w - T_\infty)},$$

$$Sh = \frac{x(q_m)}{D_B(\phi_w - \phi_\infty)}$$
(19)

where

$$\tau_w = \mu \left(\frac{\partial u}{\partial y} \right)_{y=0}$$

is the local wall shear stress,

$$(q_w)_f = -k_f \left(\frac{\partial T}{\partial y}\right)_{y=0},$$

$$(q_w)_p = -k_p \left(\frac{\partial T}{\partial y}\right)_{y=0},$$

$$(q_w)_s = -k_s \left(\frac{\partial T}{\partial y}\right)_{y=0},$$

are the heat flux at the wall for the fluid, particle, solid phases, respectively and

$$q_m = -D_B \left(\frac{\partial \phi}{\partial y}\right)_{y=0}$$

is the mass transfer coefficient.

Using the similarity transformation (eq. (12)),

$$\begin{split} &\frac{1}{2}C_{f}\sqrt{Re_{x}}=f''(0), \quad Nu_{f}/\sqrt{Re_{x}}=-\theta'_{f}(0), \\ Ν_{p}/\sqrt{Re_{x}}=-\theta'_{p}(0), Nu_{s}/\sqrt{Re_{x}}=-\theta'_{s}(0), \\ &Sh/\sqrt{Re_{x}}=-\phi'(0). \end{split} \tag{20}$$

3. Stability investigation

The non-linearity of the Navier–Stokes equations and the range of variations in fluid flow parameters admit the possibility of occurrence of more than one solution for certainly many nonlinear problems. The chosen mathematical problems feature two distinct solutions with regard to the shrinking parameter or the decelerated flow (reversed flow) situations. The solutions attributing to the decaying nature of any disturbances can be accounted to be of stable nature which can be found by analysing the nature of the obtained solutions. Merkin [36] discussed different types of solutions corresponding to boundary layers flows, such as, the regions in which the solutions ceases to exist, regions with unique solutions and regions with multiple solutions. A temporal stability analysis was made on the multiple(dual) solutions which unveiled the stability of the upper branch solutions and they are practically possible whereas the lower branch ones are unstable. A similar stability investigation of the unsteady flow situations for the mixed convective boundary layer flow with small/large suction effects was done by Weidman et al [37]. A pioneering work on the linear stability exploration for two thermal state problems streamed over wedge domains was performed by Gogate et al [38]. There has been no primary work on the stability investigation of the heat flow solutions which forms an important criterion in this study since the three-phase thermal non-equilibrium assumptions give a different flow pattern for different interphase parameters. Here we interpret the stable behaviour of both the solutions for the fluid flow, energy equations for the fluid, particle and solid phases and the concentration equations.

The time-dependent similarity variables are given in following form:

$$\eta = y\sqrt{\frac{a}{v_f(1-ct)}}, \quad \tau = \frac{at}{1-ct},$$

$$u = \frac{ax}{1-ct}\frac{\partial f}{\partial \eta}(\eta, \tau), \quad v = -\sqrt{\frac{av_f}{1-ct}}f(\eta, \tau),$$

$$\theta_f(\eta, \tau) = \frac{T_f - T_\infty}{T_w - T_\infty}, \quad \theta_p(\eta, \tau) = \frac{T_p - T_\infty}{T_w - T_\infty},$$

$$\theta_s(\eta, \tau) = \frac{T_s - T_\infty}{T_w - T_\infty}, \quad \Phi = \frac{\phi - \phi_\infty}{\phi_w - \phi_\infty}.$$
(21)

Extracting the similarity transformed form of eqs (4)–(9) using the newly defined variables (eq. (21)),

$$\frac{\partial^{3} f}{\partial \eta^{3}} \left(1 + \beta_{0} \left(\frac{\partial^{2} f}{\partial \eta^{2}} \right)^{2} \right) + 1 + A - \Lambda \left(\frac{\partial f}{\partial \eta} - 1 \right)$$

$$+Ri[\theta_{f} - Nr\Phi] - \frac{1}{\epsilon} A \left[\frac{\partial f}{\partial \eta} + \frac{\eta}{2} \frac{\partial^{2} f}{\partial \eta^{2}} \right]$$

$$-(1 + A\tau) \frac{1}{\epsilon} \frac{\partial^{2} f}{\partial \eta \partial \tau} - \frac{1}{\epsilon^{2}} \left[\left(\frac{\partial f}{\partial \eta} \right)^{2} - f \frac{\partial^{2} f}{\partial \eta^{2}} \right] = 0,$$

$$(22)$$

$$\frac{1}{Pr} \frac{\partial^{2} \theta_{f}}{\partial \eta^{2}} - A \frac{\eta}{2} \frac{\partial \theta_{f}}{\partial \eta} + \frac{1}{\epsilon} f \frac{\partial \theta_{f}}{\partial \eta} + \frac{1}{\epsilon} \theta_{f} \frac{\partial f}{\partial \eta} + A\theta_{f}$$

$$+Nb \frac{\partial \theta_{f}}{\partial \eta} \frac{\partial \Phi}{\partial \eta} + Nt \left(\frac{\partial \theta_{f}}{\partial \eta} \right)^{2} + N_{HP}(\theta_{p} - \theta_{f})$$

$$+N_{HS}(\theta_{s} - \theta_{f}) - (1 + A\tau) \frac{\partial \theta_{f}}{\partial \tau} = 0,$$

$$(23)$$

$$\frac{\epsilon_{p}}{Pr} \frac{\partial^{2} \theta_{p}}{\partial \eta^{2}} - A \frac{\eta}{2} \frac{\partial \theta_{p}}{\partial \eta} + \frac{1}{\epsilon} f \frac{\partial \theta_{p}}{\partial \eta} + \frac{1}{\epsilon} \theta_{p} \frac{\partial f}{\partial \eta} + A\theta_{p}$$

$$-\gamma_{p} N_{HP}(\theta_{p} - \theta_{f}) - (1 + A\tau) \frac{\partial \theta_{p}}{\partial \tau} = 0,$$

$$(24)$$

$$\frac{\epsilon_{s}}{Pr} \frac{\partial^{2} \theta_{s}}{\partial \eta^{2}} - A \frac{\eta}{2} \frac{\partial \theta_{s}}{\partial \eta} + A\theta_{s} - \gamma_{s} N_{HS}(\theta_{s} - \theta_{f})$$

$$-(1 + A\tau) \frac{\partial \theta_{s}}{\partial \tau} = 0,$$

$$(25)$$

$$\frac{1}{Le} \left(\frac{\partial^{2} \Phi}{\partial \eta^{2}} + \frac{Nt}{Nb} \frac{\partial^{2} \theta_{f}}{\partial \eta^{2}} \right) - A \frac{\eta}{2} \frac{\partial \Phi}{\partial \eta} + \frac{1}{\epsilon} f \frac{\partial \Phi}{\partial \eta}$$

$$-(1 + A\tau) \frac{\partial \Phi}{\partial \tau} = 0,$$

$$(26)$$

and the boundary conditions are

$$f(0,\tau) = 0, \quad \frac{\partial f}{\partial \eta}(0,\tau) = \lambda, \quad \theta_f(0,\tau) = 1,$$

$$\theta_p(0,\tau) = 1, \quad \theta_s(0,\tau) = 1, \quad \Phi(0,\tau) = 1,$$

$$\frac{\partial f}{\partial \eta}(\eta,\tau) \to 1, \quad \theta_f(\eta,\tau) \to 0, \quad \theta_p(\eta,\tau) \to 0,$$

$$\theta_s(\eta, \tau) \to 0, \quad \Phi(\eta, \tau) \to 0 \text{ as } \eta \to \infty.$$
 (27)

Upon assuming linearity in the stability analysis, the perturbation expansion for the steady-state solution employing Merkin [36] and Weidman *et al* [37] is given by

$$F(\eta, \tau) = e^{\gamma \tau} (f(\eta, \tau) - f_0(\eta)),$$

$$H_f(\eta, \tau) = e^{\gamma \tau} (\theta_f(\eta, \tau) - \theta_{f0}),$$

$$H_p(\eta, \tau) = e^{\gamma \tau} (\theta_p(\eta, \tau) - \theta_{p0}),$$

$$H_s(\eta, \tau) = e^{\gamma \tau} (\theta_s(\eta, \tau) - \theta_{s0}),$$

$$N(\eta, \tau) = e^{\gamma \tau} (\Phi(\eta, \tau) - \Phi_0),$$
(28)

where τ is the dimensionless time variable, γ represents the corresponding eigenvalues of the governing problem (eqs (4)–(9)), $f_0(\eta)$ satisfies the governing steady-state problem and $F(\eta)$ is assumed to be relatively smaller than $f_0(\eta)$.

The linearisation yields

$$(1 + \beta_0 f_0''^2) \frac{\partial^3 F}{\partial \eta^3} + \left(\frac{f_0}{\epsilon^2} - \frac{A\eta}{2\epsilon} + 2Af_0'' f_0'''\right) \frac{\partial^2 F}{\partial \eta^2} + \left(\frac{\gamma}{\epsilon} - \frac{A}{\epsilon} - \frac{2f_0'}{\epsilon^2} - \Lambda\right) \frac{\partial F}{\partial \eta} + \frac{1}{\epsilon^2} f_0'' F + Ri H_f - Ri Nr N + \frac{A\gamma\tau}{\epsilon} \frac{\partial F}{\partial \eta} - \frac{(1 + A\tau)}{\epsilon} \frac{\partial^2 F}{\partial \eta \partial \tau} = 0, \quad (29)$$

$$\frac{1}{Pr} \frac{\partial^{2} H_{f}}{\partial \eta^{2}} + \left(\frac{f_{0}}{\epsilon} - \frac{1}{\epsilon} \frac{\partial f_{0}}{\partial \eta} - \frac{A\eta}{2}\right) \frac{\partial H_{f}}{\partial \eta} + (\gamma - A)H_{f}$$

$$+ \frac{F}{\epsilon} \frac{\partial \theta_{f0}}{\partial \eta} - \frac{\theta_{f0}}{\epsilon} \frac{\partial F}{\partial \eta} + Nb \left(\frac{\partial H_{f}}{\partial \eta} \frac{\partial \Phi_{0}}{\partial \eta} + \frac{\partial \theta_{f0}}{\partial \eta} \frac{\partial N}{\partial \eta}\right)$$

$$+ 2Nt \frac{\partial \theta_{f0}}{\partial \eta} \frac{\partial H_{f}}{\partial \eta} + A\gamma\tau H_{f} + N_{HP}(H_{p} - H_{f})$$

$$+ N_{HS}(H_{s} - H_{f}) - (1 + A\tau) \frac{\partial H_{f}}{\partial \tau} = 0, \tag{30}$$

$$\begin{split} &\frac{\epsilon_{p}}{Pr}\frac{\partial^{2}H_{p}}{\partial\eta^{2}} + \left(\frac{f_{0}}{\epsilon} - \frac{1}{\epsilon}\frac{\partial f_{0}}{\partial\eta} - \frac{A\eta}{2}\right)\frac{\partial H_{p}}{\partial\eta} \\ &+ (\gamma - A)H_{p} + \frac{F}{\epsilon}\frac{\partial\theta_{p0}}{\partial\eta} - \frac{\theta_{p0}}{\epsilon}\frac{\partial F}{\partial\eta} + A\gamma\tau H_{p} \\ &- \gamma_{p}N_{HP}(H_{p} - H_{f}) - (1 + A\tau)\left(\frac{\partial H_{p}}{\partial\tau}\right) = 0, \quad (31) \end{split}$$

$$\frac{\epsilon_s}{Pr} \frac{\partial^2 H_s}{\partial \eta^2} - \frac{A\eta}{2} \frac{\partial H_s}{\partial \eta} + (\gamma - A)H_s + A\gamma\tau H_s$$

$$-\gamma_s N_{HS}(H_s - H_f) - (1 + A\tau) \left(\frac{\partial H_s}{\partial \tau}\right) = 0, \quad (32)$$

$$\frac{1}{Le} \frac{\partial^2 N}{\partial \eta^2} + \left(\frac{f_0}{\epsilon} - \frac{A\eta}{2}\right) \frac{\partial N}{\partial \eta} - \gamma N + \frac{F}{\epsilon} \frac{\partial \Phi_0}{\partial \eta}$$

$$+\frac{1}{Le}\frac{Nt}{Nb}\frac{\partial^{2}H_{f}}{\partial\eta^{2}} + A\gamma\tau N - (1+A\tau)\frac{\partial N}{\partial\tau} = 0,$$
(33)

satisfying

$$\eta = 0, \tau \ge 0 : F = 0, \frac{\partial F}{\partial \eta} = 0, H_f = 0,$$

$$H_p = 0, H_s = 0, N = 0,$$
(34)

$$\eta \to \infty, \tau \ge 0 : \frac{\partial F}{\partial \eta} \to 0, H_f(\eta, \tau) \to 0,$$

$$H_p \to 0, H_s \to 0, N \to 0. \tag{35}$$

The eigenvalue problem eqs ((29)–(34)) furnishes an innumerable set of eigenvalues $\gamma_1 < \gamma_2 < \gamma_3 < \cdots$, wherein the smallest eigenvalue γ_1 is obtained for testing the nature of disturbances (exponentially growing/decaying). If the smallest eigenvalue assumes a positive value, then the solutions possess an initially decaying behaviour of disturbances showing stable characteristics while for negative γ_1 , the solutions possess unstable characteristics. The above equations are transformed to yield the eigenvalue problem by considering $\tau=0$, the steady-state problem as follows:

$$(1 + \beta_{0} f_{0}^{"2}) F_{0}^{"'} + \left(\frac{f_{0}}{\epsilon^{2}} - \frac{A\eta}{2\epsilon} + 2Af_{0}^{"} f_{0}^{"'}\right) F_{0}^{"}$$

$$+ \left(\frac{\gamma}{\epsilon} - \frac{A}{\epsilon} - \frac{2f_{0}^{\prime}}{\epsilon^{2}} - \Lambda\right) F_{0}^{\prime} + \frac{1}{\epsilon^{2}} f_{0}^{"} F_{0}$$

$$+ Ri H_{f0} - Ri Nr N_{0} = 0, \qquad (36)$$

$$\frac{1}{Pr} H_{f0}^{"} + \left(\frac{f_{0}}{\epsilon} - \frac{f_{0}^{\prime}}{\epsilon} - \frac{A\eta}{2}\right) H_{f0}^{\prime} + (\gamma - A) H_{f0}$$

$$+ \frac{F_{0}}{\epsilon} \theta_{f0}^{\prime} - \frac{F_{0}^{\prime}}{\epsilon} \theta_{f0} + Nb (H_{f0}^{\prime} \Phi_{0}^{\prime} + \theta_{f0}^{\prime} N_{0}^{\prime}) + Nt \theta_{f0}^{\prime} H_{f0}^{\prime}$$

$$+ N_{HP} (H_{p0} - H_{f0}) + N_{HS} (H_{s0} - H_{f0}) = 0, \qquad (37)$$

$$\frac{\epsilon_{p}}{Pr} H_{p0}^{"} + \left(\frac{f_{0}}{\epsilon} - \frac{f_{0}^{\prime}}{\epsilon} - \frac{A\eta}{2}\right) H_{p0}^{\prime} + (\gamma - A) H_{p0}$$

$$+ \frac{F_{0}}{\epsilon} \theta_{p0}^{\prime} - \frac{F_{0}^{\prime}}{\epsilon} \theta_{p0} - \gamma_{p} N_{HP} (H_{p0} - H_{f0}) = 0, \qquad (38)$$

$$\frac{\epsilon_{s}}{Pr} H_{s0}^{"} - \frac{A\eta}{2} H_{s0}^{\prime} + (\gamma - A) H_{s0}$$

$$- \gamma_{s} N_{HS} (H_{s0} - H_{f0}) = 0, \qquad (39)$$

$$\frac{1}{Le} N_{0}^{"} + \left(\frac{f_{0}}{\epsilon} - \frac{A\eta}{2}\right) N_{0}^{\prime} + \gamma N_{0} + \frac{F_{0}}{\epsilon} \Phi_{0}^{\prime}$$

$$+ \frac{1}{Le} \frac{Nt}{Nb} H_{f0}^{"} = 0, \qquad (40)$$

satisfying

At
$$\eta = 0$$
: $F_0(0) = 0$, $F'_0(0) = 0$, $H_{f0}(0) = 0$, $H_{p0}(0) = 0$, $H_{s0}(0) = 0$, $H_{s0}(0) = 0$, $H_{s0}(0) = 0$,

As
$$\eta \to \infty$$
: $F_0(\eta) \to 0$, $F'_0(\eta) \to 0$, $H_{f0}(\eta) \to 0$,
 $H_{n0}(\eta) \to 0$, $H_{s0}(\eta) \to 0$, $N_0(\eta) \to 0$. (41)

The above eigenvalue problem is solved for the selected range of different parameters in the varying range like Pr, Le, Ri, Nr, etc. For solving the problem, we impose new conditions on $F_0(\eta)$, $H_{f0}(\eta)$, $H_{p0}(\eta)$, $H'_{s0}(0)$ and $N_0(\eta)$.

4. Results and discussion

The similarity transformed equations (eqs (13)–(17)) holding eq. (19) is computationally solved using the Matlab software. The asymptotic boundary conditions provided by eq. (19) is approximated by considering finitely large value for η (here, $\eta = 15$) which will be sufficient to attribute to the fully developed flow and the missing slopes at $\eta = 0$ are guessed. In this problem, multiple(dual) solution profiles obtained with unique guesses for each of the solutions exist satisfying the asymptotic boundary conditions. The present numerical results are compared with the solutions obtained by Naganthran et al [39] for different values of material parameter (β_0) and the shrinking parameter λ which are presented in table 1. The numerical validation (comparison) of the obtained results with the available literature has been portrayed. Since the numerical values are almost closer with the compared research work, it means that the obtained numerical results are valid and accurate.

Numerical results of an unsteady Hiemenz flow of a special third-grade nanofluid streaming over a perforated shrinking sheet employing tri-temperature model to represent an LTNE are discussed. The asymptotic boundary conditions are satisfied for two different initial values thereby obtaining two different solution profiles. Multiple(dual) solutions are obtained for the flow properties with varying physical parameters. It can be understood that multiple solutions are found to exist when the velocity of the wall acts along opposite directions [40]. It is also interesting to note that the range of shrinking parameter to yield dual solutions is influenced by the unsteadiness parameter and the suction parameter [41]. Moreover, the flow of the third-grade fluid considered in this study follows non-Newtonian behaviour wherein both the normal and shear stresses differ from the corresponding stresses of a Newtonian fluid. Until now, there is no way to find the range of physical parameters to identify the range of physical parameters for which multiple solutions exist. One of the most effective approach is to find the exponentially decaying solutions and identify the stable solutions. By using the stability analysis, we find that the first

of the dual profiles corresponds to a stable and physically interpretative one whereas the other one is unstable and unusually physically deviating. The representative results for the velocity, temperature of the fluid, particle and solid phases and particle concentration are provided graphically and in tabular form for various flow controlling parameters such as material parameter (β_0) , porous permeability parameter A, Brownian motion parameter Nb, thermophoresis parameter Nt, buoyancy ratio parameter Nr, Lewis number Le, Prandtl number Pr, interface heat transfer coefficient N_{HP} and N_{HS} , modified thermal capacity ratio parameter γ_p and γ_s and modified thermal diffusivity ratio parameter ϵ_p and ϵ_s . The fixed parameters are unsteady parameter A, Richardson number Ri, porosity parameter ϵ and shrinking parameter λ .

In figures 2–9 we observe that there exists dual solutions, one corresponds to the stable and physically realisable one represented by the solid lines and the second branch of solutions, though satisfy the asymptotic boundary conditions are, in general, not physically interpretable (represented by dashed lines). The variation in β_0 (the non-Newtonian parameter) with the dimensionless velocity $f'(\eta)$ is depicted in figure 2. Increase in β_0 leads to an increase in the momentum boundary layer for the stable solutions (upper branch solutions) whereas unstable solutions (lower branch solution) have a reverse effect. The analysis of stable solutions conveys that the shear stress decreases with the increase in β_0 . This was also observed by Abbasbandy and Hayat [28], where the analysis was conducted for both suction and injection. Particularly, we see that although many parameters influence the change in boundary layer formation, the impact of injection parameter is able to control the shear behaviour in boundary layer flows. Figure 3 elucidates that a rise in Λ decreases the obstruction in the fluid flow (may be due to increase in pore size) which results in enhancing the permeable flow of momentum. Figure 4 shows that the variations of Nb and Nt lead to a rise in velocity, thereby decreasing the boundary layer thickness for the upper branch solution and the adjoint lower branch solution there occurs an increase in velocity. This is because the increase in the micro-convection levels induces a faster motion of interacting particles, hence increasing the velocity. Figure 5 shows that an increase in fluid/particle and fluid/solid modified thermal diffusivity ratio (ϵ_p, ϵ_s) increases the velocity of the flow for both upper branch and lower branch solutions.

The influence of β_0 on the dimensionless fluid temperature θ_f , nanoparticle temperature θ_p and solid phase temperature θ_s are plotted in figures 6, 7 and 8, respectively. Increase in material parameter results in small enhancement in the temperature profile of all the phases (fluid, particle and solid) and this effect can be hardly

Pramana – J. Phys. (2024) 98:132 Page 13 of 16 132

seen for the upper branch solution whereas for the lower branch solution, the increase leads to an abnormal reduction in the temperature for all the phases and the related thermal boundary layers. The influence of β_0 on nanoparticle volume fraction (Φ) is shown in figure 9 with dual solutions. It is clear from figure 9 that nanoparticle concentration is increased for larger values of β_0 for the upper branch solution. In the case of lower branch solution, initially the nanoparticle concentration of the flow increases with an increase in β_0 but after certain distance the nanoparticle concentration of the fluid flow starts decreasing. Hence, the nanoparticles tend to increase the boundary layer to a small extent.

The unstable and unaccountable physical nature of the lower branch solutions make us to proceed for results with the stable (upper branch solution). Moreover, by envisaging the unstable solutions, the impact of the stable solutions in the corresponding figures cannot be understood easily. Therefore, figures 10-19 represent only the upper branch solutions. The effect of Nield numbers (N_{HP}, N_{HS}) is plotted in figure 10. It is found that for the smallest value of Nield numbers $N_{HP} = N_{HS} = 0.1$ (nearly 0) the convective heat transport between the fluid-solid and fluid-nanoparticle phase is very small. It is interesting to note that as N_{HP} and N_{HS} approach zero, there occurs only a negligible heat transport between the fluid-particle and the fluidsolid interphases. Hence, the nanoparticle and solid matrix almost fail in convective heat transport. Hence we observe for smaller values of Nield number, the temperature of the solid seems to be very high and the difference between the solid, fluid and nanoparicles seems to be vital. Further, for intermediate values of Nield number $N_{HP} = N_{HS} = 1$ as depicted in figure 10b, the difference between the phases reduces when compared with the last one. The thermal boundary layer of the fluid, particle increases and that of the solid phase decreases and the difference seems to be more subtle for $N_{HS} = N_{HP} = 100$ and the difference almost diminishes for the highest value of Nield numbers $N_{HS} = N_{HP} = 100$. It is signified that as N_{HP} and N_{HS} approaches larger values such as 100, 1000 and even more, the three distinct phases (fluid, particle and solid) behave like a single phase and can be regarded as the LTE state. This phenomenon shows that there is a shift from LTNE to LTE as the Nield number increases due to the highest convective heat transfer. The effect of the fluid-particle and fluid-solid modified thermal capacity ratios (γ_p, γ_s) on the temperature profile is sketched in figure 11. It is shown that the results are similar to the results obtained for the Nield numbers. The transformation from the local thermal non-equilibrium state to the local thermal equilibrium state is observed as γ_p , γ_s increase from 0.1 to 1000. This reveals that as $\gamma_p, \gamma_s \to \infty$, local thermal equilibrium is achieved. For brevity, the results of the fluid–particle and fluid–solid modified thermal diffusivity ratios ϵ_p , ϵ_s on the temperature profile are omitted as the results obtained are similar to the results in figure 11.

The influence of β_0 with varying porous permeability parameter (Λ) on local Nusselt number is sketched in figures 12, 13, 14 and 15. The increase in β_0 leads to a decrease in local Nusselt number for all the three phases, while the Sherwood number is observed to increase near the wall. Figures 16, 17 and 18 show the effect of local Nusselt number near the wall with respect to Brownian motion and thermophoresis parameter for different values of material parameter. The combined effect of random motions of colliding nanoparticles induced by Brownian motion and nanoparticle motion due to thermal gradient caused by thermophoresis increases the finer distribution of heat, thereby reducing local Nusselt number for the fluid, particle and solid phases near the wall. Figure 19 portrays that larger values of Brownian motion parameter (Nb) and thermophoresis parameter (Nt) create an increase in the Sherwood number. It is observed from figures 15–18 that the local Nusselt number for all the phases decreases as β_0 increases whereas Sherwood number has a considerable increase with β_0 .

Tables 2–5 assume constant values of the physical parameters as follows: Nb = Nt = Nr = 0.1, $\gamma_p =$ $\gamma_s = s = \beta_0 = N_{HP} = N_{HS} = 1$ and $\Lambda = 2$. The smallest eigenvalues corresponding to Le = Pr =Nr = 1 are provided in table 2, in which the positive eigenvalues govern the stable solutions and the negative eigenvalues correspond to the unstable solutions. Numerical results of the physical quantities such as local Nusselt number for the fluid, particle and solid phases, Sherwood number and skin-friction coefficient analysed for various values of fluid-particle and fluid-solid modified thermal diffusivity ratio parameters (ϵ_p , ϵ_s) are presented in tables 3–5. Table 3 shows that the rate of heat transfer of the fluid and particle phases decreases with an increase in fluid-particle and fluid-solid modified thermal diffusivity ratio parameters when Pr = 1. Heat transfer rate of the solid increases with an increase in ϵ_p , ϵ_s which can also be interpreted as the decrease in the thermal boundary layer of the solid phase. Skin friction coefficient is an increasing function of ϵ_p , ϵ_s . As Pr increases to 2, we observe that local Nusselt number of both the fluid and particle phases increases and that of the solid phase decreases. Upon increasing Pr, a decrease in skin-friction coefficient and Sherwood number is noticed. This implies that the Brownian motion of the nanosized particle plays a significant role in affecting the thermal behaviour of the nanoparticles.

The variation of the fluid–particle and fluid–solid modified thermal diffusivity ratio parameters (ϵ_p, ϵ_s)

132 Page 14 of 16 Pramana – J. Phys. (2024) 98:132

Table 1. Comparison of numerical results with Naganthran *et al* [39] for f''(0) for various values of λ and β_0 when s = 3, A = -1, $\epsilon = \Lambda = 1$ and Ri = 0.

eta_0		f''(0)						
		Present results		Naganthran et al [39]				
	λ	First solution	Second solution	First solution	Second solution			
1	-1.5	2.193764	-1.282856	2.1937	-1.2828			
	-1	2.166657	-1.722114	2.1666	-1.7221			
	0	2.044786	-2.014235	2.0448	-2.0142			
2	-1.5	1.496962	-0.776318	1.4969	-0.7763			
	-1	1.555901	-1.190562	1.5558	-1.1906			
	0	1.476849	-1.413027	1.4768	-1.4130			

Table 2. Smallest eigenvalue γ_1 for varied range of λ when Pr = Le = Nr = 1.

λ	Upper solution	Lower solution	
-1.5	0.0812	-0.0312	
-1	0.1173	-0.0976	
0	0.2853	-0.1833	
1	0.4754	-0.3094	
1.5	0.6548	-0.4006	

Table 3. Numerical results of f''(0), $-\theta'_f(0)$, $-\theta'_p(0)$, $-\theta'_s(0)$ and $-\Phi'(0)$ for different values of Pr, ϵ_p and ϵ_s when Le=Nr=1.

Pr	ϵ_p	ϵ_{s}	f"(0)	$-\theta_f'(0)$	$-\theta_p'(0)$	$-\theta'_s(0)$	$-\Phi'(0)$
1	0.1	0.1	2.965228	2.959132	33.937394	-2.633585	1.432302
	0.4	0.4	2.965618	2.907704	8.171023	0.021597	1.495041
	0.9	0.9	2.966100	2.828162	3.613177	0.565947	1.583342
2	0.1	0.1	2.954505	5.806345	70.907714	-3.244948	-1.579950
	0.4	0.4	2.956118	5.512951	17.227949	-0.520636	-1.258468
	0.9	0.9	2.956554	5.390375	7.453788	0.292099	-1.127964

Table 4. Numerical results of f''(0), $-\theta'_f(0)$, $-\theta'_p(0)$, $-\theta'_s(0)$ and $-\Phi'(0)$ for different values of Le, ϵ_p and ϵ_s when Pr = Nr = 1.

Le	ϵ_p	$\epsilon_{\scriptscriptstyle S}$	f''(0)	$-\theta_f'(0)$	$-\theta_p'(0)$	$-\theta'_s(0)$	$-\Phi'(0)$
1	0.1	0.1	2.965228	2.959132	33.937394	-2.633585	1.432302
	0.4	0.4	2.965618	2.907704	8.171023	0.021597	1.495041
	0.9	0.9	2.966100	2.828162	3.613177	0.565947	1.583342
2	0.1	0.1	2.966598	2.900303	33.942281	-2.629759	4.985963
	0.4	0.4	2.966978	2.849627	8.172199	0.022038	5.050761
	0.9	0.9	2.967447	2.772320	3.613650	0.566113	5.137146

Table 5. Numerical results of f''(0), $-\theta'_f(0)$, $-\theta'_p(0)$, $-\theta'_s(0)$ and $-\Phi'(0)$ for different values of Nr when $\epsilon_p = \epsilon_s = Pr = Le = 1$.

Nr	f"(0)	$-\theta_f'(0)$	$-\theta_p'(0)$	$-\theta'_s(0)$	$-\Phi'(0)$
0.1	2.966196	2.815518	3.276047	0.609211	1.597767
0.5	2.952193	2.814460	3.274959	0.609152	1.598375
0.9	2.938081	2.813396	3.273865	0.609093	1.598986

Pramana – J. Phys. (2024) 98:132 Page 15 of 16 132

for different Lewis number is depicted in table 4. We can see that there is no notable variation in all physical parameters for varying Le, except for the Sherwood number, which has a significant increase by varying Le. Numerical results of the physical quantities, such as Nusselt number, Sherwood number and skin-friction coefficients, are analysed for different values of Nr and Pr and given in table 5. As Nr increases, the convective heating tends to get stronger which makes the heat transfer rate at the wall to become weaker.

5. Conclusion

The objective of this work is the time-dependent analysis of the impinging flow of a special third-grade nanofluid streaming over a perforated shrinking sheet using the local thermal non-equilibrium approach. The numerical results of the boundary layer flow characteristics for the velocity, temperature of the fluid, particle and solid phases and mass concentration as well as reduced skin-friction coefficient, local Nusselt number and local Sherwood number are presented graphically and in tabular form for various combinations of the physical parameters. The main points are summarised as follows:

- Dual solutions are obtained when the unsteadiness is negative, one of which is stable and the other one is unstable.
- Momentum boundary layer increases with increasing material parameter whereas increases with increasing porous parameter, Brownian motion and thermophoresis parameter.
- Temperature distribution and nanoparticle concentration are increased by increasing the material parameter.
- Sherwood number directly augments with porous parameter, Brownian motion and thermophoresis parameter whereas Nusselt number for the fluid, particle and solid phases decreases with porous parameter, Brownian motion and thermophoresis parameter.
- Smaller values of inter-phase heat transfer parameters $(N_{HP}, N_{HS} \rightarrow 0)$ and modified thermal capacity ratios $(\gamma_p, \gamma_s \rightarrow 0)$ enhance the thermal non-equilibrium effect.

Acknowledgement

Author P Gayathri would like to thank PSG College of Arts & Science-SEED Fund for the financial support.

References

- [1] P X Jiang, Z P Ren and B X Wang, *Numer. Heat Transf.* (*Part A*) **35**, 99 (1999)
- [2] A Nouri-Borujerdi, A R Noghrehabadi and D A S Rees, *Trans. Porous Media* **69**, 281 (2007)
- [3] F Wu, W Zhou and X Ma, *Int. J. Heat Mass Transfer* **85**, 756 (2015)
- [4] A Omara, A Bourouis and S Abboudi, J. Appl. Fluid Mech. 9, 223 (2016)
- [5] P Montienthong, P Rattanadecho and W Klinbun, *Int. J. Heat Mass Transfer* **106**, 720 (2017)
- [6] Y Y Chen, B W Zhang and Z D Qian, *Int. Commun. Heat Mass Transfer* **95**, 80 (2018)
- [7] M R Salimi, M Taeibi-Rahni and H Rostamzadeh, *Int. J. Therm. Sci.* **153**, 106348 (2020)
- [8] A Chakravarty, N Biswas, K Ghosh, N K Manna, A Mukhopadhyay and S Sen, *J. Therm. Anal Calorim.* **143**, 3741 (2021)
- [9] S Pati, A Borah, M P Boruah and P R Randive, *Int. Commun. Heat Mass Transfer* **132**, 105889 (2022)
- [10] H Nemati, V Souriaee, M Habibi and K Vafai, *Numer. Heat Transfer, Part A: Appl.* **84**(11), 1323 (2023)
- [11] K Hiemenz, Dingler Polytech. J. 326, 321 (1911)
- [12] W A Khan and I Pop, J. Thermophys. Heat Transfer 26, 681 (2012)
- [13] M N Sadiq, B Sarwar, M Sajid and N Ali, J. Therm. Anal. Calorim. 147, 5199 (2022)
- [14] Advancements in nanotechnology for energy and environment edited by D Tripathi, R K Sharma and H F Öztop (Springer, 2022)
- [15] Nanomaterials and nanoliquids: Applications in energy and environment edited by D Tripathi, R K Sharma, H F Öztop and R Natarajan (Springer Nature, 2023)
- [16] S R Gomari, R Alizadeh, A Alizadeh and N Karimi, *Numer. Heat Transfer* **75**, 647 (2019)
- [17] J Akram, N S Akbar and D Tripathi, *Arab. J. Sci. Eng.* **47(6)**, 7487 (2022)
- [18] P K Mandal, G S Seth, S Sarkar and A Chamkha, J. Therm. Anal. Calorim. 143, 1901 (2021)
- [19] J Prakash, R Balaji, D Tripathi, A K Tiwari and R K Sharma, *Adv. Nanotechnol. Ener. Environ.* (Springer, Singapore, 2022). https://doi.org/10.1007/978-981-19-5201-2_14
- [20] I Waini, A Ishak and I Pop, *Int. Commun. Heat Mass Transfer* **130**, 105804 (2022)
- [21] P Rana, S Gupta and G Gupta, *Int. Commun. Heat Mass Transfer* **134**, 106025 (2022)
- [22] A V Kuznetsov and D A Nield, Trans. Porous Media 83, 425 (2010)
- [23] B S Bhadauria and S, Agarwal, *Trans. Porous Media* 88, 107 (2011)
- [24] H Vaidya, K V Prasad, D Tripathi, R Choudhari, Hanumantha and H Ahmad, *BioNanoScience* **13(4)**, 2348 (2023)
- [25] X Jiang, H Zhang and S Wang, Phys. Fluids 32, 113105 (2020)

132 Page 16 of 16 Pramana – J. Phys. (2024) 98:132

[26] R J P Gowda, H M Baskonus, R N Kumar, B C Prasannakumara and D G Prakasha, *Int. J. Appl. Comp. Math* **7**, 109 (2021)

- [27] J Prakash, A Sharma and D Tripathi, *Pramana J. Phys.* **94**, 1 (2020)
- [28] S Abbasbandy and T Hayat, Commun. Nonlinear Sci. Numer. Simul. 16, 3140 (2011)
- [29] T Hayat, S Nawaz, A Alsaedi and B Ahmad, Euro. Phys. J. Plus 135(5), 1 (2020)
- [30] Y M Chu, M I Khan, N B Khan, S Kadry, S U Khan, I Tlili and M K Nayak, *Int. Commun. Heat Mass Transfer* **118**, 104893 (2020)
- [31] A W Ogunsola, R A Oderinu and A D Ohaegbue, *Int. J. Activ. Energy* **43(1)**, 8792 (2022)
- [32] M Turkyilmazoglu, Eur. Phys. J. Plus 136, 376 (2021)
- [33] S Shukla and U Gupta, *J. Heat Transfer* **144(9)**, 092501 (2022)
- [34] R L Fosdick and K R Rajagopal, *Arch. Ration. Mech. Anal.* **70**, 145 (1979)

- [35] M Pakdemirli, Int. J. Eng. Sci. 32, 141 (1994)
- [36] J H Merkin, J. Eng. Math. 20, 171 (1985)
- [37] P D Weidman, D G Kubittschek and A M J Davis, *Int. J. Eng. Sci.* 44, 730 (2006)
- [38] S P Gogate, M C Bharathi and R B Kudenetti, *J. Heat Transfer* **143(4)**, 041802 (2021)
- [39] K Naganthran, R Nazar and I Pop, *Sci. Rep.* **6**(1), 24632 (2016)
- [40] P K Kameswaran, P Sibanda, C Ram Reddy and P V Murthy, *Boundary Value Problems* **2013**, 1 (2013)
- [41] N Bachok, A Ishak and I Pop, *Int. J. Heat Mass Transfer* **55(7–8)**, 2102 (2011)